

# MAXIMALLY SEPARATED AVERAGES PREDICTION FOR HIGH FIDELITY REVERSIBLE DATA HIDING

*Dibakar Hazarika, Sobhan Kanti Dhara, and Debashis Sen*

Department of Electronics and Electrical Communication Engineering,  
Indian Institute of Technology, Kharagpur, India

## ABSTRACT

Recently pixel pairing and pixel sorting/selection have been used in prediction-error expansion based reversible data hiding schemes to generate low entropy prediction-error histograms (PEH) necessary for achieving high fidelity. Such schemes generally use the four-neighbor average rhombus predictor as it allows pixel sorting and flexible pixel pairing. In this paper, we propose the maximally separated averages (MSA) predictor that uses the four-neighborhood context. It can replace the rhombus predictor in pixel pairing and sorting based schemes for lowering PEH entropy further to achieve higher performance. At each pixel location, we choose the two maximally separated average values and decide either on using one of them as the predicted value or on avoiding prediction at the pixel location. This is based on the observation that the prediction-error sequence entropy decreases with the increase in the separation between the two average values. Experimental results demonstrate that the state-of-the-art schemes achieve considerable performance improvement by using the proposed MSA predictor.

**Index Terms**— Reversible data hiding, prediction-error expansion, maximally separated averages prediction

## 1. INTRODUCTION

Content fidelity is an important concern in information security and has led to the development of numerous solutions for the issues of copyright protection, covert communication, and authentication [1]–[6]. The state-of-the-art approach for preventing unintended use of a digital medium is to hide or embed information into it for integrity protection and authentication. The use of conventional data hiding approaches for this purpose leads to permanent distortion of the digital medium. This is undesirable in the case of highly content sensitive applications such as military and medical image processing [4], [5] where permanent distortion of the digital medium is unacceptable. To meet the security needs of such applications, reversible data hiding (RDH) [7] techniques can be used which allow exact recovery of the original digital medium after extraction of the hidden data.

An RDH technique has two objectives which must be simultaneously realized. Firstly, the embedded data must be imperceptible to the user. Secondly, the modifications due to data embedding must be reversible so that the original medium can be losslessly recovered. Therefore, given a cover medium and a payload (secret data), the goal of an RDH technique is to minimize the embedding distortion due to the reversible modifications. The various techniques developed so far for RDH in images can be organized into three categories: (1) compression based methods [8]–[10], (2) histogram modification based methods including histogram shifting (HS) [11]–[13], difference expansion (DE) [14], [15] and prediction-error expansion (PEE) [16]–[27], and (3) integer transform based methods [28]–[30].

The PEE technique, first proposed in [16], is one of the most extensively explored technique among the aforementioned techniques. Most PEE techniques consist of two steps. In the first step, a sequence of prediction-errors (PE) is derived by predicting the pixels in the cover image using the neighboring pixels and computing the PEs. In the second step, the payload bits are reversibly embedded into the PE sequence by modifying its histogram, commonly referred to as the prediction-error histogram (PEH). The PEH shape plays a significant role in the performance (minimization of embedding distortion) of PEE [20], [22]. Due to the spatial correlation among the image pixels, the PEH is centrally distributed around the histogram bin containing the zero PEs. Usually, the PEs in the first few most populated PEH bins are used for embedding data. The PEs in the other PEH bins are not used for data embedding but are modified to make the embedding process reversible which also contribute to increase in embedding distortion [20]. Therefore, the performance of PEE depends upon the increasing the concentration of the PEs in a few histogram bins rather than having the PEs distributed in a large number of histogram bins. In other words, for achieving better performance using PEE, a PE sequence with low entropy, i.e., a sharply distributed PEH (also referred to as a low entropy PEH) is desirable.

Several approaches have been devised for achieving low entropy PEHs. The prediction accuracy based approaches [17]–[19] focus on devising high accuracy prediction strategies for obtaining low entropy PEHs. The pixel sorting or pixel selection based techniques [20]–[25], and [27], achieve low entropy PEHs by excluding the rough pixels, which are more likely to generate PEs with high magnitude, from the aforementioned two steps of PEE. The pixel pairing based techniques [24], [25], and [27] pair up pixels to form low entropy two dimensional (2D) PEHs. The underlying assumption is that if correlated pixels are paired, the two PEs in each pixel pair are likely to be similar leading to a 2D PEH with lower entropy as compared to the corresponding 1D PEH.

The recent pixel pairing and pixel sorting based scheme [27] exhibits better performance than the other aforementioned schemes [17]–[25]. This can be attributed to the efficient adaptive pixel pairing strategy and the adaptive 2D PEH modification used in [27]. The recent high performance scheme [27] and most of the other pixel sorting and pixel pairing based schemes [20], [21], [24], and [25] use the four-neighbor average (rhombus) predictor, introduced in [20], as it allows pixel sorting and flexible pixel pairing. The local least square (LLS) predictor, proposed in [18], has better prediction accuracy than the rhombus predictor. However, the performance of the RDH scheme in [18] is not as good as [27] as the embedding framework used in [18] is very basic. While using the LLS predictor, the PE computed at a pixel location is required to be modified before the PE at the next pixel location can be calculated. Therefore, the LLS predictor cannot be easily incorporated into schemes that employ pixel sorting and pixel pairing such as [24], [25], and [27].

The multi-predictor sorting and selection mechanism (MPSSM), proposed in [19], allows multiple predictors to be combined for increasing prediction accuracy. In MPSSM, a pixel location is either not predicted at all or the output of one of the predictors is chosen as the predicted value. However, the prediction contexts of the predictors combined using MPSSM in [19] are incompatible with the four-neighbor (rhombus) prediction context (see Fig. 1(a)) commonly used in pixel sorting and pixel pairing based schemes. As a result, these predictors combined using MPSSM cannot be used directly in such schemes. Therefore, an efficient low entropy PEH generating predictor, that can be substituted for the rhombus predictor in the pixel sorting and pixel pairing schemes including the high performance scheme of [27], is desirable. This would allow such schemes to exploit the benefits of both low entropy prediction, and pixel sorting and pixel pairing to achieve improved performance.

In this paper, we propose a novel maximally separated averages (MSA) predictor which generates PE sequences with considerably lower entropy as compared to the rhombus predictor. The proposed predictor uses the four-neighbor prediction context and can be readily incorporated into any pixel sorting and pixel pairing based scheme (that uses rhombus predictor) for exploiting the benefits of both low entropy prediction, and pixel sorting and pixel pairing. Using the four-neighbor pixels, eleven ( ${}^4C_2 + {}^4C_3 + {}^4C_4$ ) different groupings can be formed and eleven different averages can be obtained by computing the means of these eleven pixel groupings. For predicting a pixel location, the proposed predictor chooses the two averages that have the maximum separation between them and then uses a simplified adaptation of the multi-predictor sorting and selection mechanism (MPSSM) [19] to either select one of the two averages as the predicted value or avoid predicting at that pixel location. We refer to the avoided pixel locations as unpredictable pixel locations (UPL). We also present an analysis which shows that the PE sequence entropy in the proposed predictor has an inverse relation with the number of UPLs and the number of UPLs has a direct relation with the separation between the two averages chosen. This justifies the use of the maximally separated averages for generating low entropy PE sequences. To validate its effectiveness, the proposed predictor is substituted for the rhombus predictor on three state-of-the-art schemes including [20], [24], and the recent high performance scheme of [27]. Experimental results demonstrate that the state-of-the-art schemes achieve considerable performance gain by using the proposed predictor in place of the rhombus predictor.

The contribution of this paper is the maximally separated averages predictor for generating low entropy PE sequences which is based on the following novelties.

- (1) The concept of using two out of the possible eleven different averages from the four-neighbor pixels to either predict a pixel location or avoid predicting at a pixel location (UPL).
- (2) A novel analysis which shows that the PE sequence entropy has an inverse relation with the number of UPLs and the number of UPLs has a direct relation with the separation between the two averages used.
- (3) Leveraging the maximally separated averages of the four-neighbor pixels for achieving low PE sequence entropy.

The rest of the paper is organized as follows. The proposed predictor is discussed in details in Section 2. The experimental results are presented and discussed in Section 3. Finally, conclusions are drawn in Section 4.

## 2. MAXIMALLY SEPARATED AVERAGES PREDICTION

### 2.1. The proposed predictor

As mentioned earlier, the proposed maximally separated averages (MSA) predictor is designed to use the four-neighbor prediction context so that it can be incorporated into any pixel sorting and pixel pairing based scheme employing the rhombus predictor. Let  $x$  be the to-be-predicted pixel value and let  $v_n, v_s, v_w,$  and  $v_e$  be its four neighbor pixels as shown in Fig. 1(a). Using the four neighbor pixels, eleven ( ${}^4C_2 + {}^4C_3 + {}^4C_4$ ) different groupings can be formed and eleven different averages can be obtained by computing the means of these eleven pixel groupings. Let a grouping containing  $k$  pixels be referred to as a  ${}^4C_k$  grouping and its average be referred to as a  ${}^4C_k$  average. The  ${}^4C_2$  averages at a pixel location can be derived using Eq. (1) as shown below.

$$\begin{aligned} v_{ns} &= [(v_n + v_s)/2] & v_{we} &= [(v_w + v_e)/2] \\ v_{ne} &= [(v_n + v_e)/2] & v_{sw} &= [(v_s + v_w)/2] \\ v_{nw} &= [(v_n + v_w)/2] & v_{se} &= [(v_s + v_e)/2]. \end{aligned} \quad (1)$$

It can be seen in Eq. (1) that the number of common pixels between any two  ${}^4C_2$  groupings is either zero or one. It can also be shown that the number of common pixels between a  ${}^4C_{k_1}$  grouping where  $k_1 \in \{2, 3, 4\}$  and another  ${}^4C_{k_2}$  grouping where  $k_2 \in \{3, 4\}$  is at least one. Hence, at any pixel location, two of the six  ${}^4C_2$  averages will be the most separated (maximally separated) among the eleven different averages and can be derived using Eq. (2).

$$\begin{aligned} v_L &= \min(v_{ns}, v_{we}, v_{ne}, v_{sw}, v_{nw}, v_{se}) \\ v_H &= \max(v_{ns}, v_{we}, v_{ne}, v_{sw}, v_{nw}, v_{se}). \end{aligned} \quad (2)$$

The proposed predictor considers the maximally separated averages  $v_L$  and  $v_H$  as the outputs of two distinct predictors and uses Eq. (3) to either select one of the two averages as the predicted value  $\hat{x}$  or avoid predicting at that pixel location. Eq. (3) is a simplified adaptation of the multi-predictor sorting and selection mechanism (MPSSM)[19].

$$\hat{x} = \begin{cases} v_H & x \geq v_H, \\ v_L & x < v_L, \\ \text{Do not predict} & \text{otherwise.} \end{cases} \quad (3)$$

The pixel locations where prediction is avoided, referred to as the unpredictable pixel locations (UPL), are not used in the subsequent steps of PEE. The preference of the maximally separated averages in the proposed predictor over the other nine averages is for increasing the number of UPLs to achieve low PE sequence entropy which is elaborated in the next section. The steps for predicting a pixel location using the proposed MSA predictor are as follows:

- Step 1. Compute the six  ${}^4C_2$  averages using Eq. (1).
- Step 2. Determine the maximally separated averages  $v_L$  and  $v_H$  using Eq. (2).
- Step 3. Determine the predicted value  $\hat{x}$  using the to-be-predicted pixel value  $x$  using Eq. (3).

### 2.2. An analysis of PE sequence entropy reduction

In this section, we present an analysis which shows that 1) the PE sequence entropy in the MSA predictor is less than that in the rhombus predictor 2) the number of UPLs has an inverse relation with the

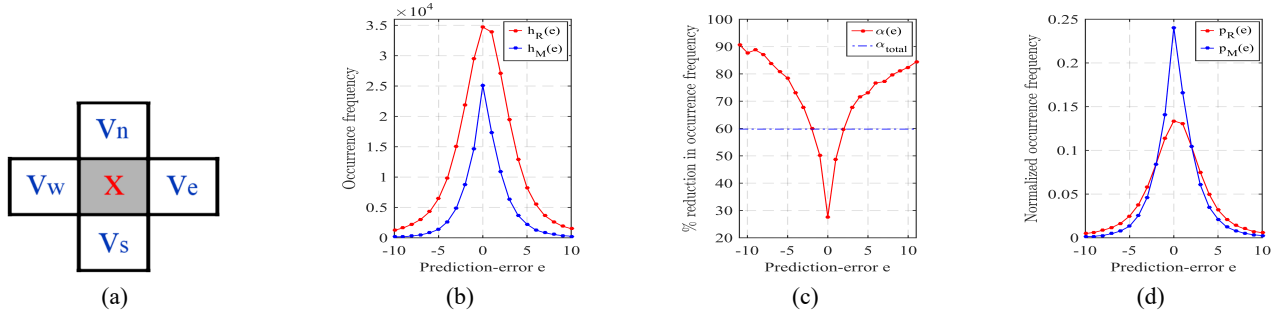


**Fig. 1.** (a) Four-neighbor (rhombus) prediction context, (b) unnormalized PEHs of rhombus and the proposed MSA predictor, (c) percentage reduction of PEs in the MSA predictor, and (d) normalized PEHs of rhombus and the MSA predictor

PE sequence entropy and 3) the separation between the two averages used in Eq. (3) has a direct relation with the number of UPLs and this justifies the use of the maximally separated averages.

Let  $h_R(e)$  and  $h_M(e)$  be the PEHs of the rhombus predictor and the MSA predictor, respectively, derived from the image *Lena*. The plots of  $h_R(e)$  and  $h_M(e)$  are illustrated in Fig. 1(b). Due to avoidance of prediction at the UPLs, the occurrence frequencies of the PEs are observed to be relatively less in case of the MSA predictor, i.e.,  $h_M(e) < h_R(e)$ . Let us consider  $\alpha(e) = 100(h_R(e) - h_M(e))/h_R(e)$  which is the percentage reduction in occurrence frequency of PEs in the MSA predictor with respect to the rhombus predictor. It can be observed from Fig. 1(b) that as the PE magnitude  $|e|$  increases from zero,  $h_R(e)$  decreases and this decrement is significant as compared to the corresponding change in  $h_R(e) - h_M(e)$ . Therefore,  $\alpha(e)$  is minimum at  $e = 0$  and barring a few local inconsistencies,  $\alpha(e)$  increases with increase in the PE magnitude  $|e|$  as shown in Fig. 1(c). Let  $\alpha_{\text{total}}$  be the percentage reduction in the total number of PEs in the MSA predictor with respect to rhombus predictor. It is obvious that  $\alpha(0) < \alpha_{\text{total}} < \max_e \alpha(e)$ . Let  $p_R(e)$  and  $p_M(e)$  be the normalized PEHs, i.e., the PE probability distributions, derived from the image *Lena* using the rhombus predictor and the MSA predictor, respectively, as illustrated in Fig. 1(d). For a PE, if  $\alpha(e) < \alpha_{\text{total}}$  ( $\alpha(e) > \alpha_{\text{total}}$ ), then  $p_M(e) > p_R(e)$  ( $p_M(e) < p_R(e)$ ). This results in the  $p_M(e)$  shape shown in Fig. 1(d) which indicates that the PE sequence entropy in the MSA predictor would be less than that in the rhombus predictor. Such empirical observations can be made in other images as well.

It can be seen in Eq. (3) that UPLs are pixel locations where  $v_L \leq x < v_H$ . This implies that the likelihood of a pixel location being an UPL is dependent on the separation  $|v_L - v_H|$  at that location. Therefore, the number of UPLs generated over the entire cover image has a direct relation with the separation between the average values used in Eq. (3).

The rhombus predictor can be considered as the case where the  ${}^4C_4$  average is used in place of both  $v_L$  and  $v_H$  in Eq. (3). Let  $U_R$  and  $U_M$  be the sets of UPLs generated in the cover image in case of the rhombus and MSA predictors, respectively. According to the relation between the separation between the average values and the number of UPLs,  $U_R = \phi$  and  $U_R \subseteq U_M$ . Based on the above analysis of Fig. 2, the use of MSA predictor in place of rhombus predictor introduces an additional set of UPLs  $U_M - U_R$  which leads to relatively lower entropy in the MSA predictor. Now, let us consider the case where two arbitrary averages  $v_a$  and  $v_b$  other than the maximally separated averages are used in Eq. (3). The separation  $|v_a - v_b|$  would be less than maximum separation  $|v_L - v_H|$  and  $v_a$  and  $v_b$  would lie within

the interval  $[v_L, v_H]$ . Therefore, if the corresponding set of UPLs is  $U_{ab}$  then  $U_R \subseteq U_{ab}$  and  $U_{ab} \subseteq U_M$ . So, based on the above analysis of Fig. 2, the use of the maximally separated averages in Eq. (3), rather than any two other arbitrary averages  $v_a$  and  $v_b$ , introduces an additional set of UPLs  $U_M - U_{ab}$  which leads to relatively lower entropy in the MSA predictor. This justifies our use of the maximally separated averages in Eq. (3) for achieving low PE sequence entropy.

### 3. EXPERIMENTAL RESULTS

The proposed MSA predictor can be incorporated into any RDH scheme that uses the four-neighbor prediction context to derive low entropy PE sequences and hence, achieve better performance. In order to demonstrate its effectiveness, we chose to incorporate the MSA predictor into the recent high performance state-of-the-art scheme [27] and two other state-of-the-art schemes [20], [24] that employ the rhombus predictor. The peak signal-to-noise ratio (PSNR), widely used in image RDH, is used as the evaluation metric for embedding distortion [7]. We have used the standard 512 x 512 test images used in [28] for our experiments. The schemes of [20], [24], and the adaptive mapping using generic search (AMG) scheme of [27] were implemented in MATLAB. Using each scheme, two sets of PSNR-payload performance results were generated. The first set consists of PSNR-payload performances of the schemes [20], [24], and [27] while employing the rhombus predictor and are denoted by ‘Sachnev-Rhom’, ‘Pairwise-PEE-Rhom’, and ‘Hybrid-AMG-Rhom’, respectively. The second set consists of PSNR-payload performances of the schemes [20], [24], and [27] while employing the proposed MSA predictor and are denoted by ‘Sachnev-MSA’, ‘Pairwise-PEE-MSA’, and ‘Hybrid-AMG-MSA’, respectively.

The performance results are illustrated in Fig. 2 which exhibit that by substituting the rhombus predictor with the proposed MSA predictor, better performance, i.e., low embedding distortion can be achieved. This is because the PE sequence entropy in the MSA predictor is lower than that in the rhombus predictor. Due to avoidance of prediction at the UPLs, the embedding capacity, i.e., the maximum embeddable payload size of the MSA predictor is not as high as that of the rhombus predictor. However, in the embeddable payload range of the MSA predictor, the average PSNR gain over rhombus predictor in the schemes of [20], [24], and [27] are 1.19, 1.00, and 0.79 dB, respectively. The PSNR gains achieved by using the MSA predictor in the schemes [20], [24], and [27] for payloads of sizes 5 and 10 kbits are given in Table 1 and Table 2, respectively. For payloads of size 5 kbits, the average PSNR gains in [20], [24], and [27] are 1.11, 1.08, and 0.84 dB, respectively. For payloads of size 10

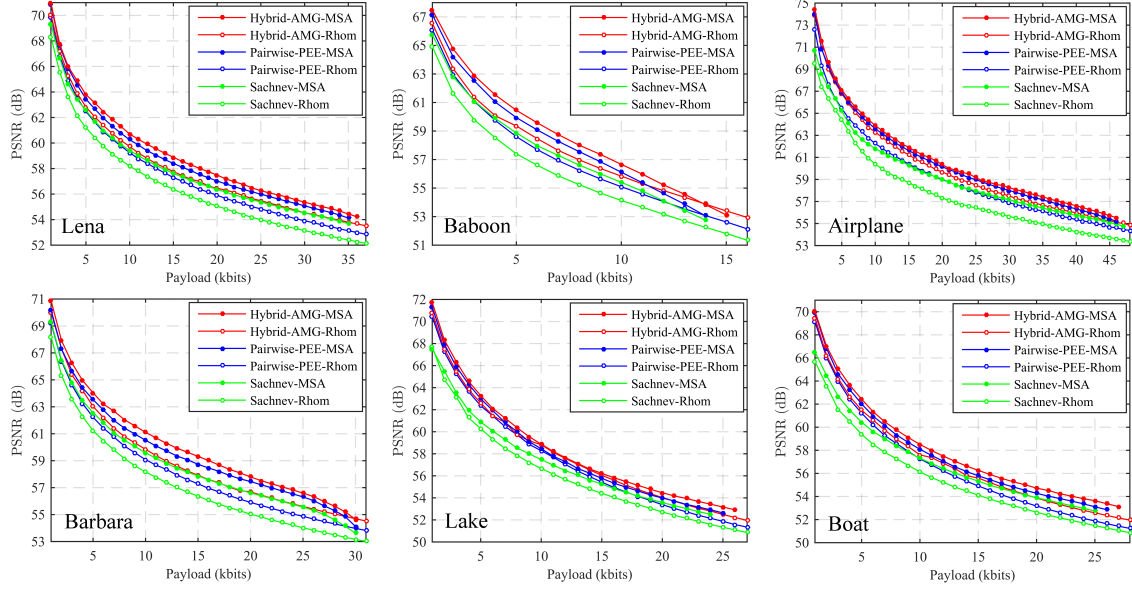


Fig. 2. PSNR-payload performance comparison between use of rhombus and MSA (proposed) predictors in the schemes [20], [24], [27].

Table 1. PSNR (in dB) comparison between the use of the rhombus predictor and the proposed MSA predictor in the schemes of [20], [24], and [27] for payloads of size 5 kbits

Images	Rhombus Predictor			MSA Predictor		
	[20]	[24]	[27]	[20]	[24]	[27]
Lena	61.20	62.48	62.82	<b>62.56</b>	<b>63.45</b>	<b>63.79</b>
Baboon	57.40	58.60	59.35	<b>58.87</b>	<b>59.94</b>	<b>60.46</b>
Airplane	64.42	65.45	66.79	<b>65.24</b>	<b>66.90</b>	<b>67.10</b>
Barbara	61.23	62.22	63.03	<b>62.56</b>	<b>63.54</b>	<b>64.04</b>
Lake	60.28	62.36	62.62	<b>60.89</b>	<b>63.00</b>	<b>63.28</b>
Boat	59.38	61.22	61.46	<b>60.43</b>	<b>62.02</b>	<b>62.43</b>
Average	60.65	62.06	62.68	<b>61.76</b>	<b>63.14</b>	<b>63.52</b>

Table 2. PSNR (in dB) comparison between the use of the rhombus predictor and the proposed MSA predictor in the schemes of [20], [24], and [27] for payloads of size 10 kbits

Images	Rhombus Predictor			MSA Predictor		
	[20]	[24]	[27]	[20]	[24]	[27]
Lena	58.20	59.24	59.73	<b>59.41</b>	<b>60.26</b>	<b>60.73</b>
Baboon	54.13	55.09	55.84	<b>55.40</b>	<b>56.11</b>	<b>56.66</b>
Airplane	60.38	62.25	63.30	<b>61.82</b>	<b>63.59</b>	<b>63.88</b>
Barbara	58.16	59.07	59.84	<b>59.59</b>	<b>60.52</b>	<b>61.11</b>
Lake	56.67	58.28	58.82	<b>57.48</b>	<b>58.46</b>	<b>58.87</b>
Boat	56.14	57.26	57.60	<b>57.30</b>	<b>58.08</b>	<b>58.51</b>
Average	57.28	58.53	59.19	<b>58.50</b>	<b>59.50</b>	<b>59.96</b>

kbits, the average PSNR gains in [20], [24], and [27] are 1.22, 0.97, and 0.77 dB, respectively.

Moreover, a comparison of PE sequence entropy for rhombus, LLS [18], and MSA predictors are shown in Table 3. It can be seen

Table 3. Comparison of entropy of prediction-error sequences

Predictor	Images					
	Lena	Babo.	Airp.	Barb.	Lake	Boat
Rhombus	4.108	5.967	3.864	5.111	4.963	4.811
LLS	3.939	5.696	3.722	<b>4.040</b>	4.869	4.432
<b>MSA</b>	<b>3.415</b>	<b>5.313</b>	<b>2.612</b>	4.337	<b>4.314</b>	<b>4.094</b>

that the proposed MSA predictor results in lower entropy as compared to the rhombus predictor which is consistent with the PSNR gains achieved in the schemes of [20], [24], and [27]. The MSA predictor is also found to be comparable in terms of entropy to the LLS predictor, which cannot be used with pixel pairing and sorting based schemes. Thus, any PEE scheme employing the rhombus predictor can improve its performance by using the proposed MSA predictor.

#### 4. CONCLUSION

In this paper, we propose a novel four-neighborhood based maximally separated averages (MSA) predictor for generating low entropy PE sequences, required for high fidelity RDH. The MSA predictor is designed to replace the rhombus predictor in the recent high performance pixel pairing and sorting based schemes for further improving their performance. At each pixel location, our predictor computes the two most separated average values using the four-neighbor pixels and either selects one of the two averages as the predicted value or considers the pixel location unpredictable. The most separated averages are used to increase the number of unpredictable pixel locations, which, based on our analysis, results in low PE sequence entropy. Experimental results demonstrate that our predictor outperforms the rhombus predictor in terms of PE sequence entropy and the state-of-the-art schemes achieve considerable performance gain by using our predictor.

## 5. REFERENCES

- [1] I. Cox, M. Miller, J. Bloom, J. Fridrich, and T. Kalker, *Digital watermarking and steganography*. Morgan kaufmann, 2007.
- [2] Y. Q. Shi, Z. Ni, D. Zou, C. Liang, and G. Xuan, "Lossless data hiding: fundamentals, algorithms and applications," in *Proceedings of the 2004 International Symposium on Circuits and Systems*, May, 2004.
- [3] R. Caldelli, F. Filippini, and R. Becarelli, "Reversible watermarking techniques: An overview and a classification," *EURASIP Journal on Information Security*, vol. 2010, p. 2, 2010.
- [4] B. Li, J. He, J. Huang, and Y. Q. Shi, "A survey on image steganography and steganalysis," *Journal of Information Hiding and Multimedia Signal Processing*, vol. 2, no. 2, pp. 142–172, 2011.
- [5] Z. Xia, X. Wang, X. Sun, and Q. Wang, "A secure and dynamic multi-keyword ranked search scheme over encrypted cloud data," *IEEE Transactions on Parallel and Distributed Systems*, vol. 27, no. 2, pp. 340–352, 2016.
- [6] J. Li, X. Li, B. Yang, and X. Sun, "Segmentation-based image copy-move forgery detection scheme," *IEEE Transactions on Information Forensics and Security*, vol. 10, no. 3, pp. 507–518, 2015.
- [7] Y.-Q. Shi, X. Li, X. Zhang, H.-T. Wu, and B. Ma, "Reversible data hiding: advances in the past two decades," *IEEE Access*, vol. 4, pp. 3210–3237, 2016.
- [8] W. Zhang, X. Hu, X. Li, and N. Yu, "Recursive histogram modification: establishing equivalency between reversible data hiding and lossless data compression," *IEEE Transactions on Image Processing*, vol. 22, no. 7, pp. 2775–2785, 2013.
- [9] X. Zhang, "Reversible data hiding with optimal value transfer," *IEEE Transactions on Multimedia*, vol. 15, no. 2, pp. 316–325, 2013.
- [10] F. Huang, X. Qu, H. J. Kim, and J. Huang, "Reversible data hiding in jpeg images," *IEEE Transactions on Circuits and Systems for Video Technology*, vol. 26, no. 9, pp. 1610–1621, 2016.
- [11] Z. Ni, Y.-Q. Shi, N. Ansari, and W. Su, "Reversible data hiding," *IEEE Transactions on Circuits and Systems for Video Technology*, vol. 16, no. 3, pp. 354–362, 2006.
- [12] X. Li, B. Li, B. Yang, and T. Zeng, "General framework to histogram-shifting-based reversible data hiding," *IEEE Transactions on Image Processing*, vol. 22, no. 6, pp. 2181–2191, 2013.
- [13] W. Zhang, X. Hu, X. Li, and Y. Nenghai, "Optimal transition probability of reversible data hiding for general distortion metrics and its applications," *IEEE Transactions on Image Processing*, vol. 24, no. 1, pp. 294–304, 2015.
- [14] J. Tian, "Reversible data embedding using a difference expansion," *IEEE Transactions on Circuits and Systems for Video Technology*, vol. 13, no. 8, pp. 890–896, 2003.
- [15] X. Li, W. Zhang, X. Gui, and B. Yang, "A novel reversible data hiding scheme based on two-dimensional difference-histogram modification," *IEEE Transactions on Information Forensics and Security*, vol. 8, no. 7, pp. 1091–1100, 2013.
- [16] D. M. Thodi and J. J. Rodríguez, "Expansion embedding techniques for reversible watermarking," *IEEE Transactions on Image Processing*, vol. 16, no. 3, pp. 721–730, 2007.
- [17] S.-L. Lin, C.-F. Huang, M.-H. Liou, and C.-Y. Chen, "Improving histogram-based reversible information hiding by an optimal weight-based prediction scheme," *Journal of Information Hiding and Multimedia Signal Processing*, vol. 4, no. 1, pp. 19–33, 2013.
- [18] I.-C. Dragoi and D. Coltuc, "Local-prediction-based difference expansion reversible watermarking," *IEEE Transactions on image processing*, vol. 23, no. 4, pp. 1779–1790, 2014.
- [19] X. Ma, Z. Pan, S. Hu, and L. Wang, "High-fidelity reversible data hiding scheme based on multi-predictor sorting and selecting mechanism," *Journal of Visual Communication and Image Representation*, vol. 28, pp. 71–82, 2015.
- [20] V. Sachnev, H. J. Kim, J. Nam, S. Suresh, and Y. Q. Shi, "Reversible watermarking algorithm using sorting and prediction," *IEEE Transactions on Circuits and Systems for Video Technology*, vol. 19, no. 7, pp. 989–999, 2009.
- [21] H. J. Hwang, H.-J. Kim, V. Sachnev, and S.-H. Joo, "Reversible watermarking method using optimal histogram pair shifting based on prediction and sorting," *KSH Transactions on Internet and Information Systems*, vol. 4, no. 4, pp. 655–670, 2010.
- [22] W. Hong, "Adaptive reversible data hiding method based on error energy control and histogram shifting," *Optics Communications*, vol. 285, no. 2, pp. 101–108, 2012.
- [23] X. Li, B. Yang, and T. Zeng, "Efficient reversible watermarking based on adaptive prediction-error expansion and pixel selection," *IEEE Transactions on Image Processing*, vol. 20, no. 12, pp. 3524–3533, 2011.
- [24] B. Ou, X. Li, Y. Zhao, R. Ni, and Y.-Q. Shi, "Pairwise prediction-error expansion for efficient reversible data hiding," *IEEE Transactions on Image Processing*, vol. 22, no. 12, pp. 5010–5021, 2013.
- [25] I.-C. Dragoi and D. Coltuc, "Adaptive pairing reversible watermarking," *IEEE Transactions on Image Processing*, vol. 25, no. 5, pp. 2420–2422, 2016.
- [26] J. Wang, J. Ni, X. Zhang, and Y.-Q. Shi, "Rate and distortion optimization for reversible data hiding using multiple histogram shifting," *IEEE Transactions on Cybernetics*, vol. 47, no. 2, pp. 315–326, 2017.
- [27] B. Ou, X. Li, W. Zhang, and Y. Zhao, "Improving pairwise pcc via hybrid-dimensional histogram generation and adaptive mapping selection," *IEEE Transactions on Circuits and Systems for Video Technology*, to be published, doi: 10.1109/TCSVT.2018.2859792.
- [28] S. Weng, Y. Zhao, J.-S. Pan, and R. Ni, "Reversible watermarking based on invariability and adjustment on pixel pairs," *IEEE Signal Processing Letters*, vol. 15, pp. 721–724, 2008.
- [29] X. Wang, X. Li, B. Yang, and Z. Guo, "Efficient generalized integer transform for reversible watermarking," *IEEE Signal Processing Letters*, vol. 17, no. 6, pp. 567–570, 2010.
- [30] F. Peng, X. Li, and B. Yang, "Adaptive reversible data hiding scheme based on integer transform," *Signal Processing*, vol. 92, no. 1, pp. 54–62, 2012.